JOURNAL OF Applied Polymer SCIENCE

Fabrication and characterization of centrifugally spun poly(acrylic acid) nanofibers

David De la Garza,[1] Francisco De Santiago,[1] Luis Materon,[2] Mircea Chipara,[3] Mataz Alcoutlabi[1]
[1]Department of Mechanical Engineering, University of Texas, Rio Grande Valley, Edinburg, Texas 78539
[2]Department of Biology, University of Texas, Rio Grande Valley, Edinburg, Texas 78539
[3]Department of Physics and Astronomy, University of Texas, Rio Grande Valley, Edinburg, Texas 78539
Correspondence to: M. Chipara (E-mail: mircea.chipara@utrgv.edu) and M. Alcoutlabi (E-mail: mataz.alcoutlabi@utrgv.edu)

ABSTRACT: The production of poly(acrylic acid) (PAA) nanofibers by the centrifugal spinning of PAA solutions in water is reported. The effect of the spinneret rotational speed and concentration of PAA solutions on the diameter of nanofibers and on their quality (assessed by the absence of beads) is discussed. The main physical properties of PAA such as glass-transition temperature (T_g) are studied in detail and compared to the feature of the as-received homopolymer. It is shown that the glass-transition temperature of the bulk PAA and PAA nanofibers (as measured by differential scanning calorimetry) depends on the heating rate according to a Williams–Landel–Ferry-like equation. Raman spectroscopy data provided additional information about the differences between the as-received polymer and the nanofibers. Preliminary results on antibacterial properties of the PAA nanofibers are reported. © 2019 Wiley Periodicals, Inc. J. Appl. Polym. Sci. **2019**, *136*, 47480.

KEYWORDS: antimicrobial; centrifugal spinning; DSC; nanofiber; poly(acrylic acid); Raman

Received 11 July 2018; accepted 9 December 2018
DOI: 10.1002/app.47480

INTRODUCTION

Polymer nanofibers have attracted increasing interest in the past decades for several applications due to their high surface area to volume ratio, flexibility, and outstanding properties compared to their bulk material counterparts. The uniqueness of these nanofibers has made them incredibly useful in many fields such as drug delivery,[1–3] tissue engineering,[1–3] energy storage,[2,4,5] wound dressing applications,[2,3] and many more. Several methods have been used to fabricate polymer nanofibers such as electrospinning,[6] melt blowing,[7] centrifugal spinning (CF),[8] coextrusion with a unique exit cutting die[9] liquid shear spinning,[10] and touch and brush spinning.[11]

Electrospinning is the most used method to produce polymer fibers due to its ability to produce fibers with diameter ranging from micrometers to nanometers (tens of nanometers to a few micrometers).[12] However, slow fiber production (~0.3 g h^{-1})[13] and the application of an electric field[6] are drawbacks to this method. An alternative to electrospinning is CFs. Forcespinning (FS), which is the trademark of CFs, was developed by Sarkar, Lozano, *et al.* at the University of Texas–Pan American and allows for the more rapid production of fibers in the nanorange and microrange by centrifugal forces.[14] This method permits the use of a larger number of polymers and composites solutions with higher concentrations to be utilized with a reduced production cost due to the use of less solvent, fast fiber production rate (1 g min^{-1}) because there is no need to apply an electric field to stretch the fibers.[14–16] Many polymer nanofibers such as: poly(ethylene oxide), polypropylene, polyvinylpyrrolidone,[14] poly-L-lactic acid,[17] polyacrylonitrile (PAN) and PAN nanocomposites,[18–20] poly (ε-caprolactone),[21] cellulose acetate,[22] and poly(ethylene terephthalate)[23] have been successfully produced by CFs for use in different applications such as energy storage, filtration, and tissue scaffolding. Polymer nanofibers have also been used for antimicrobial applications. In recent work, composite nanofibers of chitosan and silver nanoparticles were successfully produced by CFs and their antimicrobial properties were reported.[24]

In this work, poly(acrylic acid) (PAA) is herein first reported as produced by CF. PAA is a weak anionic polyelectrolyte with a hygroscopic nature and has been widely used for a variety of applications. PAA is typically mixed with other polymers in aqueous solutions and has previously been electrospun to form fibrous hydrogels due to the polymer's ability to swell in response to environmental stimuli and its changes in pH.[25] The adsorption capability of PAA allows for its use in water treatment as a metal ion scavenger and its use in disposable diapers.[26] PAA has also been used in lithium-ion batteries as a binder for better battery performance[27,28] and a recent study has been reported on the use

Additional Supporting Information may be found in the online version of this article.

of composites containing PAA for humidity sensing due to the sensitivity of PAA to humidity.[29] The antimicrobial properties of PAA together with other polymers and composites have been studied as well.[30–32] One of these particular studies conducted by Gratzl *et al.* show that PAA containing diblock copolymers exhibit antimicrobial properties displaying better results with increasing acrylic acid content.[30] In this work, PAA nanofibers are prepared by CF for use in antimicrobial applications. The morphology and thermal characterization of the PAA fibers and their bulk material counterpart are studied using different experimental techniques such as scanning electron microscope (SEM), thermogravimetric analysis (TGA), differential scanning calorimetry (DSC), and Raman spectroscopy.

EXPERIMENTAL

Materials. The materials used are PAA polymer (M_v = 450,000) purchased from Sigma-Aldrich (USA) and deionized (DI) water.

Preparation of Polymer Solutions. The PAA solutions of various concentrations (8–15 wt %) were obtained by dissolving the polymer in DI water. All solutions were homogenized by stirring for 24 h.

CF Setup. The CF method (Figure 1) uses centrifugal forces to extrude the polymer solution or melt through the needle-based spinneret to obtain nanofibers. The fiber jets were formed by high rotational speed of the spinneret. Two 30-gauge half-inch sterile needles (Fisher Scientific, USA) were inserted into the spinneret on each side and 2 mL of the precursor solution was injected into the spinneret orifice. The FS equipment was set to a spinning time of 3 min and spinneret rotational speeds varied from 4000 to 8000 rpm. Fiber samples were removed from the collectors with a microscopic glass slide for characterization tests and square fiber mats were produced for antimicrobial testing. The PAA solutions were prepared at room temperature for 24–48 h.

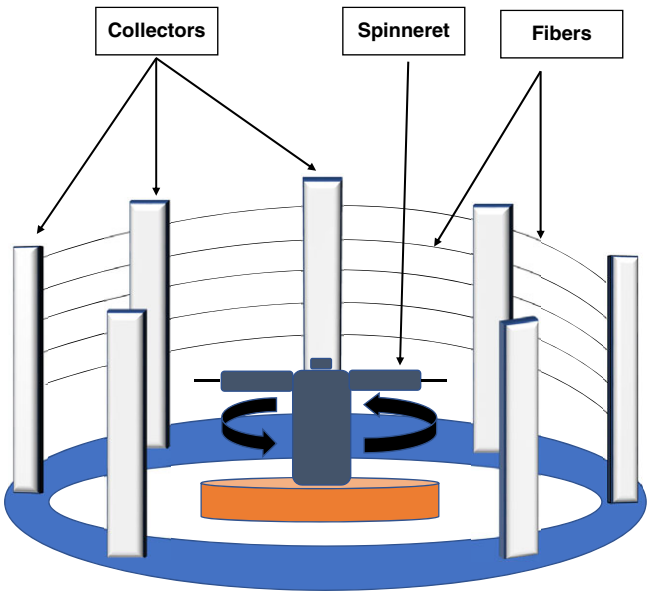

Figure 1. Schematic of the CFs method displaying the collectors, spinneret, and fiber web. [Color figure can be viewed at wileyonlinelibrary.com]

The temperature and humidity were controlled during the CF of PAA fibers. All samples were stored under vacuum at 80 °C for 24 h, in order to remove any residual water. The experiments were conducted at room temperature (22–25 °C) and a humidity between 60 and 70%.

Characterization Analysis

Scanning Electron Microscopy. The fiber morphology was examined with a Zeiss Sigma VP field emission SEM. A thin layer of gold was used to coat the samples for 30 s at 45 mA with a Desk II Denton Vacuum Sputter prior to imaging. Several SEM images were taken of each fibers sample at different regions to measure the fiber diameters and generate histograms to display the fiber diameter distribution. An average of 50–80 fibers from the SEM images were selected to measure fiber diameter with the AxioVision microscope software and a QI Macros software was used to generate the histograms.

Raman Spectroscopy. Raman measurements have been obtained by using Renishaw inVia Raman Microscope equipped with a laser diode, operating at 785 nm.

Differential Scanning Calorimetry. The thermal properties of the PAA bulk powder and nanofibers were acquired using TA Instruments, DSC Q100 (USA). To obtain thermograms for the PAA nanofibers, the DSC scans were conducted from 40 to 225 °C at heating and cooling rates of 1, 2, 5, 10, 15, 20, 25, 30, 40, 45, and 50 °C min^{-1}. All tests were completed under a nitrogen atmosphere.

Thermogravimetric Analysis. The thermal degradation of the PAA nanofibers was investigated using TA Instruments TGA Q500 under a nitrogen atmosphere. All samples were heated up to 800 °C at a heating rate of 10 °C min^{-1}.

Antimicrobial Testing. The antimicrobial testing was conducted via the Kirby–Bauer method using *Escherichia coli* and *Staphylococcus aureus* bacteria. The bacteria were grown onto a nutrient broth (1:10 ratio) and 100 μL of the bacterial suspension from the dilution was added to the surface of agar plates. An L-shaped glass rod was used to fully disperse the suspension on the plate. Half-inch circular fiber mats were placed on the surface of the agar plate and placed in an incubator at 37 °C for 24 h for further analysis.

RESULTS AND DISCUSSION

Fiber Surface Characterization: SEM Analysis. Figure 2(a) shows the SEM image for 12 wt % PAA nanofibers centrifugally spun at a spinneret rotational speed of 6000 rpm. Similar images were collected for all nanofiber samples ranging from 9 to 14 wt %. The rotational speed of the spinneret was varied from 4000 to 8000 rpm for all polymer solutions. Figures S1-S6 in the supplementary data sheet show the SEM images of PAA nanofibers spun at different concentrations (9–14 wt. %) and rotational speeds between 4000 and 8000 rpm. Sparse to no fiber formation resulted at 8 wt % and 15 wt % PAA solution concentrations as well as at a spinneret rotational speed below 4000 rpm and above 8000 rpm for all other solutions due to either an insufficient

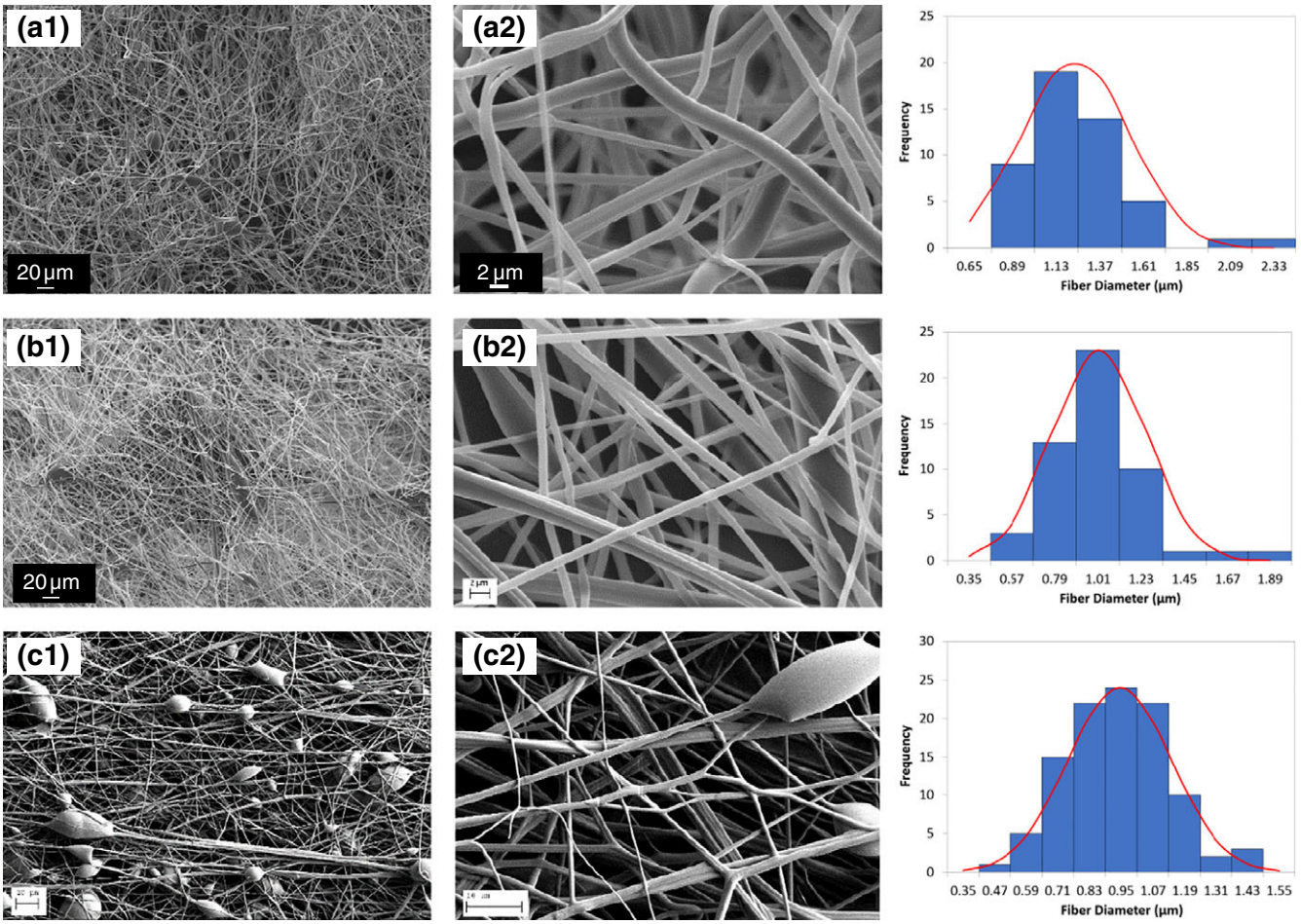

Figure 2. SEM images and fiber diameter distribution of (a) 12 wt % PAA concentration spun @ 6000 rpm, (b) 12 wt % PAA concentration spun @ 8000 rpm, and (c) 9 wt % PAA concentration spun at 4000 rpm. The SEM images were obtained at different magnifications: (A_1, B_1) 600×, (C_1) 300×, (A_2, B_2) 7000×, and (C_2) 15,000×. [Color figure can be viewed at wileyonlinelibrary.com]

ejection time of the polymer solution or limited fiber elongation and solvent evaporation. Variations in the spinneret rotational speeds played an important factor in the formation of beads and average fiber diameters. The average fiber diameter for nanofibers centrifugally spun at 6000 rpm and PAA concentration of 12 wt % was 1100 nm, while the PAA nanofibers spun at 8000 rpm with the same polymer concentration had an average fiber diameter of 900 nm [Figure 2(b)]. This is due to the stretching of the nanofibers while the solvent is evaporating as the spinning rate is increased. The 12 wt % PAA concentration was found to be optimal displaying the lowest amount of beaded fibers unlike the SEM image shown in Figure 2(c) for a 9 wt % PAA concentration where a significant amount of beads were formed after CF. As expected, lower polymer concentrations produced a smaller average fiber diameter as shown in Figure 3.[21] The figure shows the average fiber diameter as a function of PAA concentration. The PAA nanofibers were centrifugally spun at a spinneret rotational speed of 6000 rpm. The average nanofiber diameters ranged from 800 to 1400 nm as the PAA concentration was increased while the spinneret speed was kept constant at 6000 rpm. The correlation coefficient for the linear fitting was $R^2 = 0.958$.

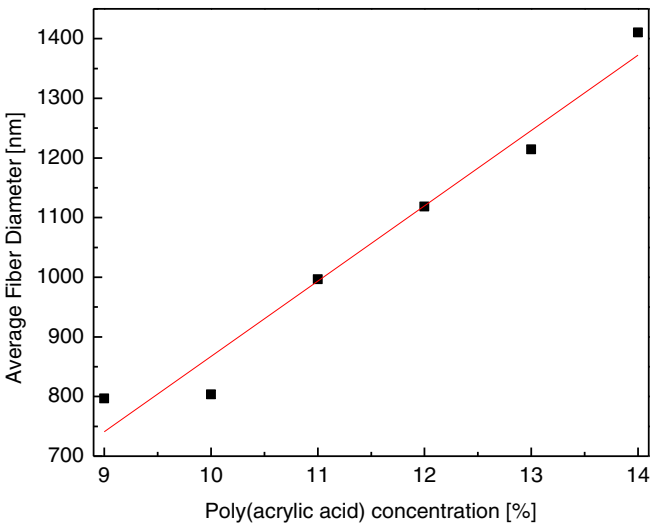

Figure 3. Average fiber diameter versus PAA concentration. The PAA fibers were forcespun at a spinneret rotational speed of 6000 rpm. [Color figure can be viewed at wileyonlinelibrary.com]

Table I. Average Fiber Diameter of PAA Fibers Centrifugally Spun at Different Spinneret Rotational Speeds (4000, 6000, and 8000 rpm) and at Different PAA Concentrations Between 9 and 14 wt %

Sample	Average fiber diameter (nm)	Standard deviation (nm)
9%-4000 rpm	884.04	195.68
9%-6000 rpm	796.60	207.92
10%-4000 rpm	942.73	245.51
10%-6000 rpm	803.74	233.04
10%-8000 rpm	860.93	241.13
11%-4000 rpm	1004.46	238.49
11%-6000 rpm	996.44	253.88
11%-8000 rpm	1010.22	331.03
12%-4000 rpm	1197.38	354.79
12%-6000 rpm	1118.37	296.14
12%-8000 rpm	906.15	239.65
13%-6000 rpm	1214.29	370.76
13%-8000 rpm	1027.55	277.43
14%-6000 rpm	1410.38	429.61
14%-8000 rpm	1380.86	393.21

As illustrated in Table I, the average fiber diameter of PAA fibers for different concentrations varied with the rotational speed of the spinneret. There is a significant effect of the polymer concentration on the average fiber diameter at each spinneret speed. The fiber diameter increases with increasing concentration. In fact, both the rotational speed of the spinneret and polymer concentration are important parameters that affect the fiber morphology and formation during CF. Figures S1-S6 in the supplementary data sheets show all the SEM images of PAA fibers spun at different PAA concentrations (9–12 wt %) and rotational speeds between 4000 and 8000 rpm.

Raman Spectroscopy. Figure 4 shows the Raman spectrum of PAA bulk and nanofibers obtained using a laser operating at 785 nm in the Raman shifts range 100–1000 cm^{-1}. Several lines were noticed and assigned as follows:

The line located at 508 cm^{-1} corresponds to bending motions of *cis* C-C=O groups. As this line is not shifted toward lower Raman shifts, it is possible to conclude that the amount of water within these nanofibers is very low.[33] Generally, the presence of water in PAA shifts some Raman lines, providing an efficient tool for the quantification of water content.[33,34] The large band observed between 613 and 645 cm^{-1} corresponds to the bending vibrations of *trans* C=O units. As this line is not shifted below 600 cm^{-1}, it is confirmed that water is not present in the nanofibers. The line at 840 cm^{-1} corresponds to symmetric vibrations in C-C=O and τ vibrations in CH_2. The position of this line confirms the lack of water. The Raman spectrum of the PAA fiber structure from 1000 to 2000 cm^{-1} is shown in Figure 5.

The line located at about 1100 cm^{-1} represents ρ motions of CH_2 units. The line at 1329 cm^{-1} reflects asymmetric of C-C=O units. This line is almost absent in PAA gels and if water is present. The line noticed at 1458 cm^{-1} is associated with the delta motions of CH_2 units and is also absent in PAA gels. The line noticed at 1669 cm^{-1} corresponds to the vibration of C=O unit. The absence of any line around 1700 cm^{-1} is an additional confirmation of the absence of water in the nanofibers.[33,35] Figure 6 shows the Raman spectrum of the PAA fibers from 2600 to 3700 cm^{-1}. The pure water Raman peak was reported at 3453 cm^{-1} and is not observed in the actual spectra.

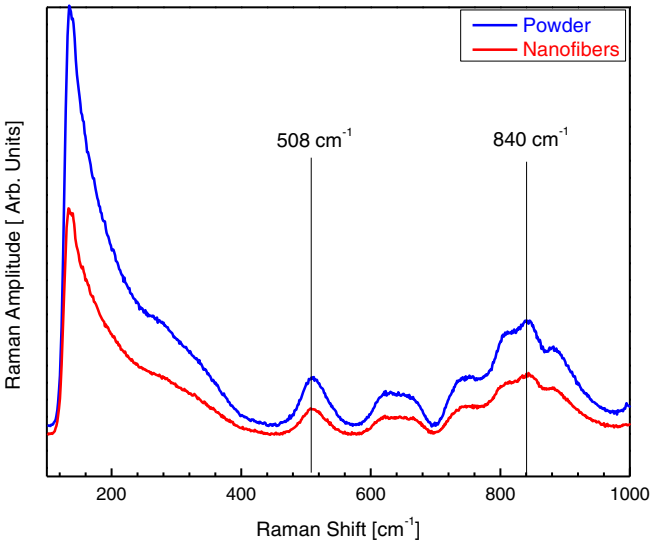

Figure 4. Raman spectra of PAA from 0 to 1000 cm^{-1}. [Color figure can be viewed at wileyonlinelibrary.com]

The Raman investigations showed that the molecular motions in PAA are not affected by the one-dimensional character of nanofiber/microfiber and consequently, within the experimental errors, the Raman spectra of PAA powder and PAA nanofibers are identical. Based on the position of Raman lines, it is concluded that the amount of adsorbed water is low (typically below 10 wt %). Furthermore, the local dynamics of PAA nanofiber/microfiber affecting the molecular

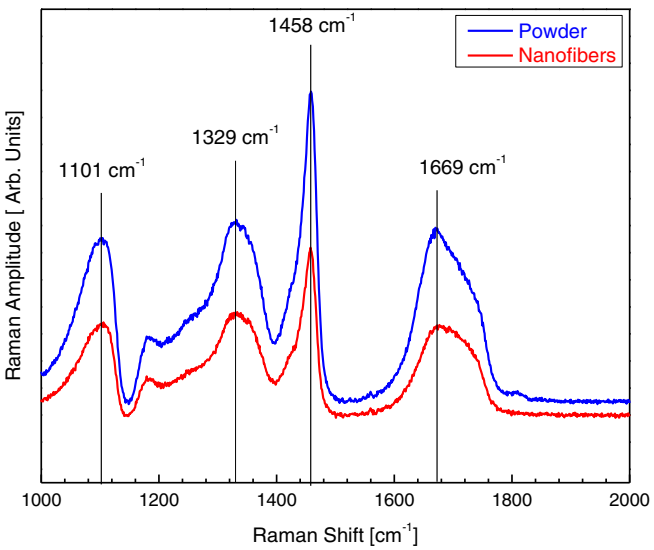

Figure 5. Raman spectra of PAA from 1000 to 2000 cm^{-1}. [Color figure can be viewed at wileyonlinelibrary.com]

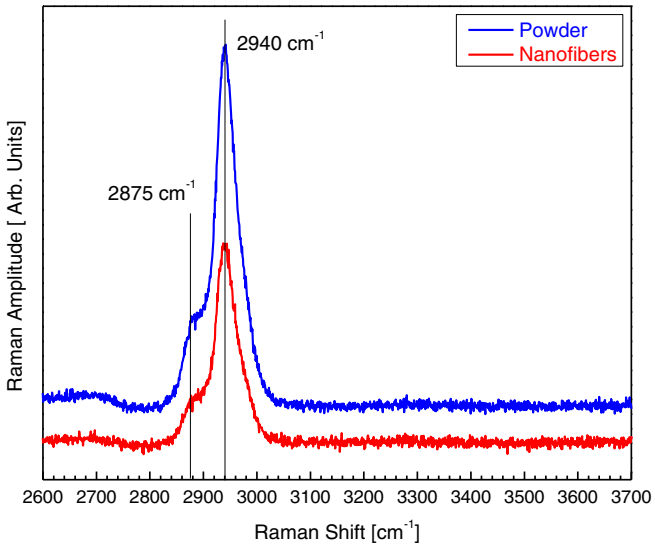

Figure 6. Raman spectra of PAA from 2600 to 3700 cm^{-1}. [Color figure can be viewed at wileyonlinelibrary.com]

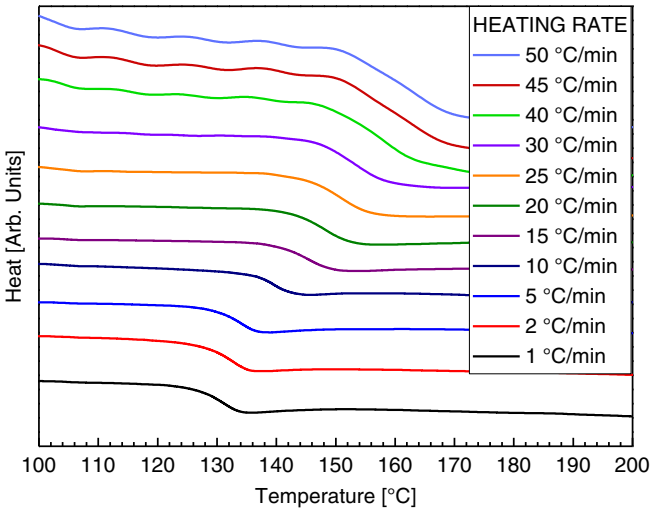

Figure 7. DSC spectra of PAA bulk at different heating rates. [Color figure can be viewed at wileyonlinelibrary.com]

polarizability was investigated in this work and is confirmed by previous studies.[33,35] It is worthwhile to mention here that water has its own Raman lines. Therefore, water can be detected by Raman spectroscopy in two ways: directly, via the Raman vibrations of water, and indirectly via modifications triggered by the water presence in PAA.

The main problem with water detection by Raman spectroscopy is caused by the experimental configuration. The Raman spectrometer that was used to conduct the experiments discussed in this work operates in the reflection mode. Technically, this makes almost impossible to use the Raman spectrometer to measure a water droplet, as the reflected laser beam is very weak and hence, the noise masks the absorption lines (however, the spectrum is nicely recorded in the transmission configuration). Consequently, the analysis was focused on the shift of some Raman lines due to the water retention within the nanofibers, which is in agreement with results reported in the literature.[33,34] This approach is not very sensitive to the presence of water and hence, relatively small amounts of water adsorbed by the polymer will not be reflected in the Raman spectrum but will be observed during TGA experiments. The estimated amount of water appears to be in the order of few weight percentages.

DSC Results. To investigate the structure and thermal properties of PAA nanofibers and bulk powder, DSC measurements have been performed at different scanning rates ranging from 1 to 50 °C min^{-1}. PAA is essentially an amorphous polymer and consequently, this study investigated the dynamics of the glass-transition temperature in bulk PAA and nanofibers of PAA.

The DSC spectra of the heating branch of bulk PAA is shown in Figure 7. It is noticed that for all heating rates, the DSC spectrum shows a sigmoidal dependence of heat flow versus temperature. The glass-transition temperature is typically defined in the middle of this dependence. However, this empirical definition is improved by defining the glass-transition temperature as the coordinate of the inflection point of the aforementioned sigmoidal dependence. Because the location of the inflection point cannot be accurately estimated, a mathematical transformation (derivative) will convert the inflection point into an extremum point, whose position is easier and more accurately estimated. Each recorded thermogram, shown in Figure 7, was numerically differentiated to obtain a graph that shows the dependence of the derivative of heat flow with respect to temperature (dH/dT). This dependence is shown in Figure 8. Similar data have been obtained for all samples at all heating rates.

Figure 9 shows the heating rate as a function of temperature for three different samples (bulk PAA, nanofibers obtained at 6000 rpm, and nanofibers obtained at 8000 rpm) at different heating rates. Each of these three curves is characterized by a single glass transition. Differences have been noticed between bulk and spun nanofibers.

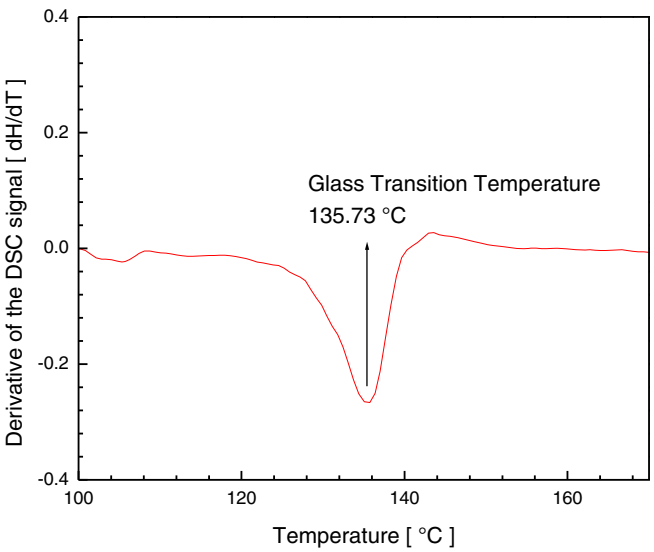

Figure 8. The derivative of the DSC scan (dH/dT) during the third heating run, displaying the glass-transition temperature as the extremum point. The DSC scans were conducted at 10 °C min^{-1} from 40 to 225 °C. The experiments were performed under nitrogen atmosphere. [Color figure can be viewed at wileyonlinelibrary.com]

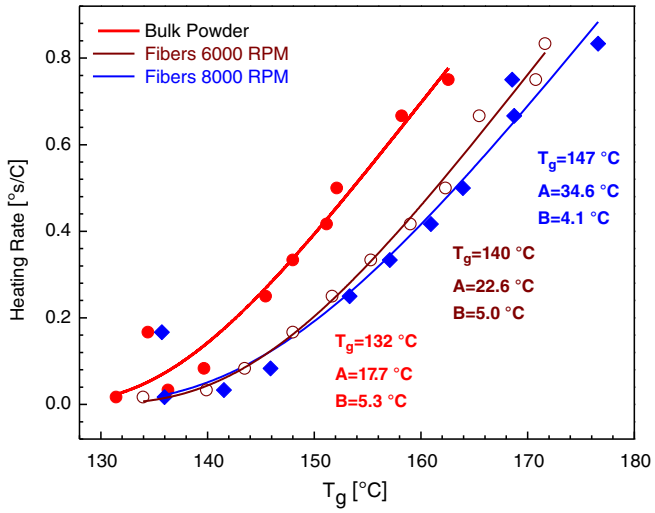

Figure 9. Heating rate versus T_g graph of bulk PAA and PAA nanofibers spun at 6000 and 8000 rpm. [Color figure can be viewed at wileyonlinelibrary.com]

The glass-transition temperatures were obtained by nonisothermal DSC measurements, at various heating rates. The DSC experiment begun with three heating–cooling cycles at a constant rate of (10 °C min^{-1}) between 25 and 250 °C, followed by 11 heating–cooling cycles at a heating rate between 1 and 50 °C min^{-1}. For each cycle, the sample was annealed for 10 min at 250 °C followed by cooling to 25 °C to start a new cycle. The second and third thermograms were identical, supporting the full erasure of the residual stresses caused by the sample preparation and processing. To improve the accuracy in the estimation of the glass-transition temperature, each DSC thermogram representing the heat flow versus temperature (at a given constant heating rate) was differentiated and the extremum point at the peak of each curve was identified as the glass-transition temperature, T_g. The values of T_g shown in Figure 9 were obtained experimentally using the aforementioned method. The experiments were done in hermetic aluminum pans. The "universal" T_g is obtained by a nonlinear fit of the data in Figure 9 using a modified Williams–Landel–Ferry (WLF).

It is observed that the glass transition of the bulk polymer (T_g = 132 °C) is lower than that for the PAA nanofibers. It is shown in Figure 9 that T_g for nanofibers increases with increasing the spinneret rotational speed (T_g = 140 °C @ 6000 rpm and T_g = 147 °C @ 8000 rpm). For all the samples, the glass transition increases as the heating rate is increased and this is a common behavior for amorphous materials.

It is very important to study the dynamics of the glass transition of the PAA fibers and PAA bulk powder based on the DSC results discussed above. We analyzed the results using WLF equation.

Time- and temperature-dependent phenomena near the glass-transition temperature and its dynamics are well described by the WLF equation:

$$\ln a_T = \frac{C_{1g}(T - T_g)}{C_{2g} + T - T_g} \quad (1)$$

where C_{1g} and C_{2g} are constants initially assumed to have universal values. It was later recognized that both C_{1g} and C_{2g} depend on the polymer nature and properties.[36] T_g is the glass-transition temperature and T is the temperature. Typically, the WLF equation is valid in the temperature range T_g + 120 K > T > T_g–C_{2g}. As noticed from the WLF equation, a_T is the shift factor and is equal to zero at $T = T_g$–C_{2g}. The shift factor, a_T, is typically the ratio between two relaxation quantities such as viscosity and relation time, for example, at a given temperature, T, the shift factor is given as: $a_T = \tau_T/\tau_{Tg} = \eta_T/\eta_{Tg}$, where τ and η are the relaxation time and viscosity, respectively. Note that in the WLF equation given above, T_g is defined as the reference temperature ($T_g = T_{ref}$). In order to use this equation to interpret the DSC data, we must recognize that the DSC experiment inspects the time–temperature map with the relaxation parameter represented by the heating rate. Consequently, a conventional value of one for the heating rate at the glass-transition temperature is assumed, which mathematically implies that a_T is proportional to the heating rate. In Figure 9, the dependence of the heating rate on temperature is represented. The best fit to the experimental data has been obtained for the expression:

$$\ln H_R \propto B\frac{(T - T_g)}{(T - T_g + A)} \quad (2)$$

where H_R is the heating rate, B is proportional to C_{1g} but not identical to C_{1g} because it was assumed that the heating rate at the glass-transition temperature is represented by one, A is identical to C_{2g}, and T_g represents the glass-transition temperature. As can be seen from Figure 9, a very good correlation between the experimental data and the predictions of the WLF-like dependence was obtained. The correlation coefficients, R^2, for the nonlinear fitting of the data for the bulk PAA powder, PAA fibers spun at 6000 and 8000 rpm, were 0.933, 0.994, and 0.954, respectively.

It is observed that the glass transition of the powder is lower than that for the fibers and that there is a slow increase in the glass-transition temperature as the spinning rate is increased. Typically, confinement effects in polymers are resulting in a decrease of the glass-transition temperature as the size of the confined medium is decreased. Microscopy data revealed a slight decrease in the diameter of the nanofibers as the spinning rate was increased. This explains the dependence of the glass-transition temperature. Parameter B is decreasing as the spinning rate was increased, while A showed an increase as the spinning rate was increased. These results indicate that the fractional free volume at T_g (which is related to B) is decreasing as the spinning rate is increased. This suggests a local order due to the stretching of the nanofiber during CF. Therefore, the fractional volume at T_g decreases as the spinning rate is increased. The increase in A suggests that the expansion coefficient decreases.

The shift of the glass temperature to higher temperatures may be a consequence of water desorption. The release of the adsorbed water and the formation of anhydride groups may also contribute to the shift of the glass-transition temperature.

It is worthwhile to mention here that the modified WLF equation [eq. (1)] allows for the estimation of the glass-transition temperature, T_g, and of the WLF constant, C_{1g}. The other WLF constant,

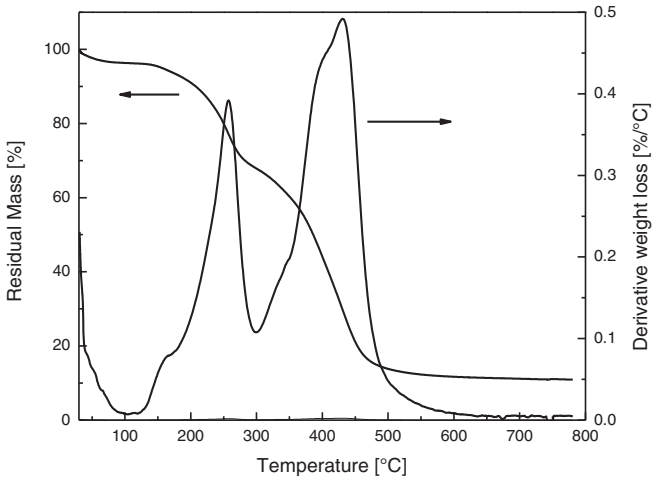

Figure 10. TGA and derivative thermogravimetric curves of the PAA fibers. The TGA thermogram was conducted in nitrogen atmosphere. The samples were heated from 25 to 800 °C at a heating rate of 10 °C min^{-1}.

C_{2g}, may be estimated up to a multiplicative constant. Further molecular modeling may be required to determine C_{1g} from such DSC data. It is known that there is a difference between a calorimetric glass transition T_g (measured by DSC) and a dynamic T_g, as observed in relaxation/creep measurements.[37–39] Studying the dynamics and thermodynamic of the glass transition in amorphous polymers and glass forming liquids is very complex and is beyond the scope of this work.

TGA Results. The thermogravimetric results of PAA microfibers are shown in Figure 10. The first derivative curve of the thermograms of PAA fibers is also shown in the figure. The TGA experiments were performed under an N_2 atmosphere. The temperature scans were conducted from 25 to 800 °C at a heating rate of 10 C min^{-1}. The TGA curve shows a total mass loss of 90% which can be divided into three steps. The first step (30–150 °C, mass loss of about 4%) is attributed to the departure of physiosorbed water and preliminary formation of anhydride groups. The second step at (~250 °C, mass loss of ~30%) is caused by the dehydration of adjacent carboxylic group to form anhydrides. The last step demonstrates the full degradation of the sample only leaving carbonaceous residue and it can be observed that there is about a 10% residual mass at 800 °C. TGA data confirmed that the amount of physiosorbed water is below 10 wt %. Based on the derivative weight loss of the PAA fibers, the most mass loss of ~30 and 46% occurs at 250 and 450 °C, respectively. Within experimental errors, we did not notice any substantial difference between TGA of nanofibers obtained at different spinning rates (between 4000 and 8000 rpm).

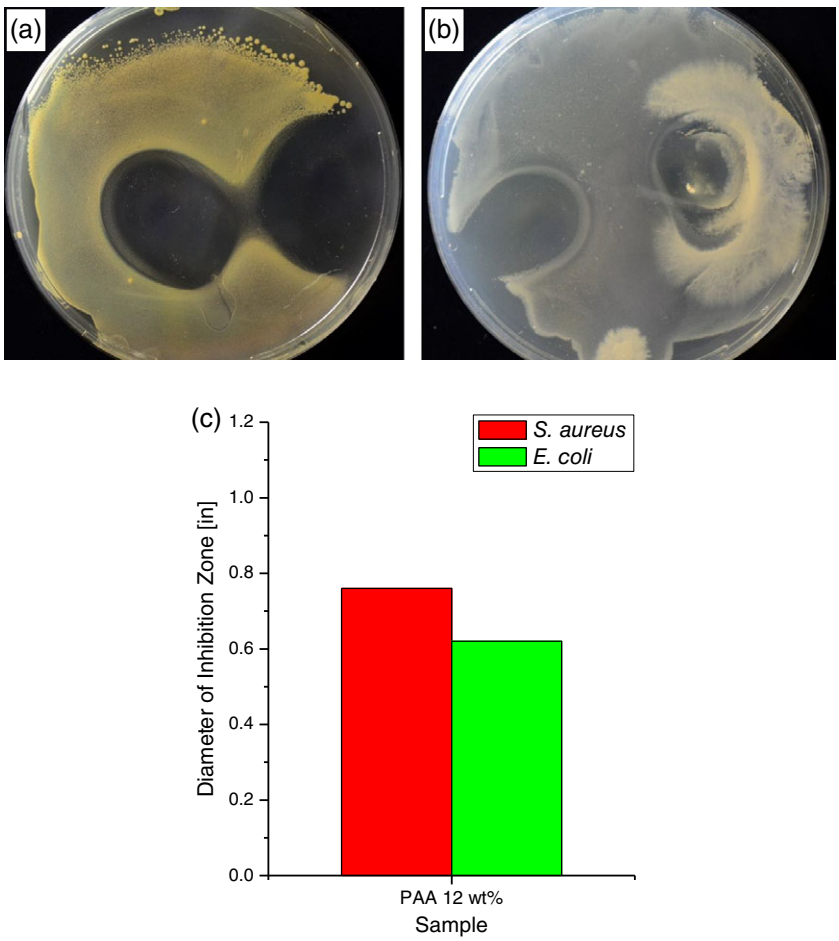

Figure 11. *In vitro* antimicrobial results of PAA nanofibers done on (a) *S. aureus* and (b) *E. coli* as well as the (c) estimated diameter of the inhibition zones. [Color figure can be viewed at wileyonlinelibrary.com]

Table II. Estimated Diameter of the Inhibition Zones for the Antibacterial/Microbial Activity Results of PAA Nanofibers Against *S. aureus and E. coli*

Fibers/bacteria system	Average diameter of the inhibition zone (in.)	Standard deviation
PAA/*S. aureus*	0.76	0.14
PAA/*E. coli*	0.62	0.07

Antimicrobial Results. The PAA fibers were tested for their antimicrobial activity. Figure 11(a,b) displays images taken of agar plates filled with both *E. coli* and *S. aureus* and the bacteria inhibition zone exhibited by the PAA nanofibers. Although the half-inch polymer nanofibers are not visible after 24 h, the clear inhibition zone exhibited by PAA is present in both the *S. aureus* and the *E. coli* agar plates. A strong antimicrobial activity in the *S. aureus* agar plate is demonstrated by a close connection of both half-inch fiber mats placed on the bacteria. However, the inhibition zone on the right section of the same plate could not be measured properly.

The PAA fibers placed on the surface of the agar plates filled with *E. coli* bacteria produced differences in antimicrobial activity. It can be noticed that inhibition is clear on the left of the plate but not on the right. Nonsterile conditions of nanofiber production and antimicrobial testing resulted in a visibly whiter portion on this particular plate which suggests that some sort of fungus grew on the pathogenic bacteria after testing. Measurements were conducted on clearer inhibition zones and Figure 11(c) shows that PAA generated a larger inhibition zone of about 0.76 in. in the Gram-negative bacteria (*S. aureus*) than in the Gram-positive bacteria (*E. coli*) with an inhibition zone of 0.62 in. The antimicrobial activity experiments against *E. coli* and *S. aureus* were performed using eight different samples made from PAA fibers (eight for *E. coli* and eight for *S. aureus*). The antimicrobial activity results shown in Figure 11 were based on the estimated average diameter of the inhibition zones of the eight PAA fiber samples. The standard deviations for the antimicrobial activity measurements of PAA fibers against *E. coli* and *S. aureus* are illustrated in Table II.

CONCLUSIONS

PAA nanofibers were fabricated for the first time by CF. The results showed an increase in nanofibers' diameter with increasing polymer concentration. A 12 wt % PAA concentration in a DI water solution was found to be the optimal concentration displaying sparse to no beaded nanofibers for three different spinneret speeds. As expected, faster spinning rates caused by higher spinneret rotational speeds decreased the fiber diameter due to the stretching of the fibers when pushed out of the needles in the CF equipment. The average fiber diameter for the 12 wt % PAA in DI water spun at 6000 rpm was 1100 nm while the average fiber diameter for the same concentration spun at 8000 rpm was 900 nm.

Detailed analysis of the Raman spectra of PAA powder and PAA nanofibers revealed that the two spectra are almost identical suggesting that there are no significant differences in the molecular motions of PAA bulk and PAA nanofibers. Additionally, the lack of Raman line shifts indicates that water is not present in PAA nanofibers. However, orientational effects have been averaged out in these measurements performed on mats of PAA nanofibers. The lack of single PAA fibers prevented us from observing potential contributions due to the stretching of the polymer.

The DSC scans conducted on PAA nanofibers demonstrated that the polymer is amorphous and glass-transition temperatures increased with increasing heating rates according to the WLF dependence for both pristine (bulk) and centrifugally spun fibers on various spinning rates.

The PAA nanofibers were tested for their antimicrobial properties and presented large inhibition zones of both Gram-positive *E. coli* and Gram-negative *S. aureus* pathogenic bacteria. Half-inch PAA fiber mats exhibited strong antimicrobial results with about 0.62 and 0.76 in. inhibition zones on *S. aureus* and *E. coli* agar plates, respectively.

ACKNOWLEDGMENTS

This research was supported by the USDA, the National Institute of Food and Agriculture, and the Integrating Food Science/Engineering and Education Network (IFSEEN) with award number: 2015-38422-24059. This work was also supported by National Science Foundation (NSF) PREM award under grant no. DMR-1523577: UTRGV-UMN Partnership for Fostering Innovation by Bridging Excellence in Research and Student Success. The authors would like to thank Hilario Cortez, Alejandro Castillo, and Thomas Eubanks from UTRGV for the SEM analysis.

REFERENCES

1. Sill, T. J.; von Recum, H. A. *Biomaterials*. **2008**, *29*(13), 1989.
2. Bhardwaj, N.; Kundu, S. C. *Biotechnol. Adv.* **2010**, *28*(3), 325.
3. Huang, Z. M.; Zhang, Y. Z.; Kotaki, M.; Ramakrishna, S. *Compos. Sci. Technol.* **2003**, *63*(15), 2223.
4. Agubra, V. A.; Zuniga, L.; Flores, D.; Villareal, J.; Alcoutlabi, M. *Electrochim. Acta*. **2016**, *192*, 529.
5. Agubra, V. A.; De la Garza, D.; Gallegos, L.; Alcoutlabi, M. *J. Appl. Polym. Sci.* **2016**, *133*(1), 42847.
6. Li, D.; Xia, Y. N. *Adv. Mater.* **2004**, *16*(14), 1151.
7. Hassan, M. A.; Yeom, B. Y.; Wilkie, A.; Pourdeyhimi, B.; Khan, S. A. *J. Membr. Sci.* **2013**, *427*, 336.
8. Zhang, X. W.; Lu, Y. *Polym. Rev.* **2014**, *54*(4), 677.
9. Du, J.; Liu, D.; Chen, S.; Wan, D.; Pu, H. *Polymer*. **2016**, *102*, 209.
10. Smoukov, S. K.; Tian, T.; Vitchuli, N.; Gangwal, S.; Geisen, P.; Wright, M.; Shim, E.; Marquez, M.; Fowler, J.; Velev, O. D. *Adv. Mater.* **2015**, *27*(16), 2642.
11. Tokarev, A.; Asheghali, D.; Griffiths, I. M.; Trotsenko, O.; Gruzd, A.; Lin, X.; Stone, H. A.; Minko, S. *Adv. Mater.* **2015**, *27*(41), 6526.
12. Pham, Q. P.; Sharma, U.; Mikos, A. G. *Tissue Eng.* **2006**, *12*(5), 1197.

13. Esmaeilzadeh, I.; Mottaghitalab, V.; Tousifar, B.; Afzali, A.; Lamani, M. *Int. J. Ind. Chem.* **2015**, *6*(3), 193.
14. Sarkar, K.; Gomez, C.; Zambrano, S.; Ramirez, M.; De Hoyos, E.; Vasquez, H.; Lozano, K. *Mater. Today*. **2010**, *13*(11), 12.
15. Lu, Y.; Li, Y.; Zhang, S.; Xu, G.; Fu, K.; Lee, H.; Zhang, X. *Eur. Polym. J.* **2013**, *49*(12), 3834.
16. Padron, S.; Fuentes, A.; Caruntu, D.; Lozano, K. *J. Appl. Phys.* **2013**, *113*(2), 024318.
17. Valipouri, A.; Ravandi, S. A. H.; Pishevar, A. R. *Fibers Polym.* **2013**, *14*(6), 941.
18. Agubra, V. A.; Zuniga, L.; De la Garza, D.; Gallegos, L.; Pokhrel, M.; Alcoutlabi, M. *Solid State Ion.* **2016**, *286*, 72.
19. Zuniga, L.; Agubra, V.; Flores, D.; Campos, H.; Villareal, J.; Alcoutlabi, M. *J. Alloys Compd.* **2016**, *686*, 733.
20. Victor, A.; Agubra, L. Z.; Flores, D.; Campos, H.; Villarreal, J.; Alcoutlabi, M. *Electrochim. Acta.* **2017**, *224*, 608.
21. Obregon, N.; Agubra, V.; Pokhrel, M. et al. *Fibers*. **2016**, *4*(2), UNSP 20, http://dx.doi.org/10.3390/fib4020020.
22. Weng, B. C.; Xu, F.; Alcoutlabi, M.; Mao, Y.; Lozano, K. *Cellul.* **2015**, *22*(2), 1311.
23. Allahkarami, M.; Bandla, S.; Winarski, R. P.; Hanan, J. C. *Appl. Surf. Sci.* **2014**, *297*, 9.
24. Cremar, L.; Gutierrez, J.; Martinez, J. et al. *Nanomed. J.* **2018**, *5*(1), 6.
25. Li, L.; Hsieh, Y. L. *Nanotechnology*. **2005**, *16*(12), 2852.
26. Kadajji, V. G.; Betageri, G. V. *Polymers*. **2011**, *3*(4), 1972.
27. Cai, Z. P.; Liang, Y.; Li, W. S.; Xing, L. D.; Liao, Y. H. *J. Power Sources*. **2009**, *189*(1), 547.
28. Park, H. K.; Kong, B. S.; Oh, E. S. *Electrochem. Commun.* **2011**, *13*(10), 1051.
29. Atchison, J.; Schauer, C. *Sensors*. **2011**, *11*, 10372.
30. Gratzl, G.; Paulik, C.; Hild, S.; Guggenbichler, J. P.; Lackner, M. *Mater. Sci. Eng. C.* **2014**, *38*, 94.
31. Serinçay, H.; Özkan, S.; Yılmaz, N.; Koçyiğit, S.; Uslu, İ.; Gürcan, S.; Arısoy, M. *Polym.-Plast. Technol. Eng.* **2013**, *52*(13), 1308.
32. Khampieng, T.; Wnek, G. E.; Supaphol, P. *J. Biomater. Sci. Polym. Ed.* **2014**, *25*(12), 1292.
33. Todica, M.; Stefan, R.; Pop, C. V.; Olar, L. *Acta Phys. Pol. A*. **2015**, *128*(1), 128.
34. Tanaka, N.; Kitano, H.; Ise, N. *Macromolecules*. **1991**, *24*(10), 3017.
35. Tsukida, N.; Muranaka, H.; Ide, M.; Maeda, Y.; Kitano, H. *J. Phys. Chem. B*. **1997**, *101*(34), 6676.
36. Williams, M. L.; Landel, R. F.; Ferry, J. D. *J. Am. Chem. Soc.* **1955**, *77*(14), 3701.
37. Alcoutlabi, M.; McKenna, G. B. *J. Phys. Condens. Matter*. **2005**, *17*(15), R461.
38. Alcoutlabi, M.; Banda, L.; McKenna, G. B. *Polymer*. **2004**, *45*(16), 5629.
39. Lee, M.; Alcoutlabi, M.; Magda, J. J.; Dibble, C.; Solomon, M. J.; Shi, X.; McKenna, G. B. *J. Rheol.* **2006**, *50*(3), 293.